Development 136, 4021-4031 (2009) doi:10.1242/dev.041129

FoxJ1-dependent gene expression is required for differentiation of radial glia into ependymal cells and a subset of astrocytes in the postnatal brain

Benoit V. Jacquet[1], Raul Salinas-Mondragon[1], Huixuan Liang[1], Blair Therit[1], Justin D. Buie[1], Michael Dykstra[2], Kenneth Campbell[3], Lawrence E. Ostrowski[4], Steven L. Brody[5] and H. Troy Ghashghaei[1,*]

Neuronal specification occurs at the periventricular surface of the embryonic central nervous system. During early postnatal periods, radial glial cells in various ventricular zones of the brain differentiate into ependymal cells and astrocytes. However, mechanisms that drive this time- and cell-specific differentiation remain largely unknown. Here, we show that expression of the forkhead transcription factor FoxJ1 in mice is required for differentiation into ependymal cells and a small subset of FoxJ1$^+$ astrocytes in the lateral ventricles, where these cells form a postnatal neural stem cell niche. Moreover, we show that a subset of FoxJ1$^+$ cells harvested from the stem cell niche can self-renew and possess neurogenic potential. Using a transcriptome comparison of *FoxJ1*-null and wild-type microdissected tissue, we identified candidate genes regulated by FoxJ1 during early postnatal development. The list includes a significant number of microtubule-associated proteins, some of which form a protein complex that could regulate the transport of basal bodies to the ventricular surface of differentiating ependymal cells during FoxJ1-dependent ciliogenesis. Our results suggest that time- and cell-specific expression of FoxJ1 in the brain acts on an array of target genes to regulate the differentiation of ependymal cells and a small subset of astrocytes in the adult stem cell niche.

KEY WORDS: Subventricular zone, Adult stem cell niche, Ependymal cells, Astrocytes, FoxJ1, Mouse

INTRODUCTION

The developing neuroepithelium consists of multipotent stem cells with radial glial features (Campbell and Gotz, 2002; Noctor et al., 2002) that give rise to various neuronal and glial cell types in the embryonic central nervous system (Rakic, 1972; Pinto and Gotz, 2007). Around the time of birth, radial glial cells are thought to differentiate into astrocytes and ependymal cells that line the cerebral ventricles in the mature brain (Schmechel and Rakic, 1979; Merkle et al., 2004; Spassky et al., 2005); however, the molecular mechanisms responsible for this differentiation are largely unknown. The differentiation into the astrocytes and ependymal cells that separate the subventricular zone (SVZ) from the fluid-filled space in the lateral ventricles is of particular interest as these cells help form an adult stem cell niche (SCN). The emergence and maintenance of the adult SCN in the SVZ is thought to support olfactory bulb (OB) neurogenesis throughout adulthood (Alvarez-Buylla and Lim, 2004).

Maintenance of adult neurogenesis is thought to depend on cellular composition within the SCN, which is compartmentalized into three functionally distinct layers. The first is an epithelial layer consisting of ependymal cells and a subset of astrocytes, both of which are in contact with the cerebrospinal fluid circulating in the lateral ventricles (Doetsch et al., 1997). The basal processes of these unique astrocytes form clusters surrounded by a few ependymal cells on the cellular lining of the ventricles (Mirzadeh et al., 2008), resembling rosette/pinwheel structures, and are organized in the developing epithelia of multiple species and organ systems (Zallen, 2007). Ependymal cells are known to influence the SCN in several ways; for example, by regulating neurogenesis through secretion of noggin (Lim et al., 2000). Furthermore, subsets of cells in this epithelial layer are thought to function as quiescent neural stem cells (Doetsch et al., 1997; Johansson et al., 1999; Spassky et al., 2005; Coskun et al., 2008) and to maintain a second layer of transit amplifying progenitors (TAPs) that proliferate rapidly (Doetsch et al., 1999a; Doetsch et al., 1999b). TAPs give rise to a third layer comprising migrating neuroblasts that travel through the rostral migratory stream (RMS) to the OB (Lois and Alvarez-Buylla, 1993; Lois and Alvarez-Buylla, 1994; Ghashghaei et al., 2007a). Upon arrival at the OB, the neuroblasts differentiate into interneurons during early postnatal and adult periods (Lois and Alvarez-Buylla, 1993; Wichterle et al., 1999). Identification of the factors required for postnatal establishment and maintenance of cellular integrity within the adult SCN is essential for deciphering functional differences between adult and embryonic regulation of neurogenesis and is crucial if the adult SCN is to be utilized in cell-based therapies.

A crucial aspect of ependymal cell differentiation is ciliogenesis. Cilia are evolutionarily conserved structures that are classified as motile or primary (Mitchell, 2004). Motile cilia depend on molecular motors and a central microtubule pair for their motility, whereas primary cilia are specialized as environmental sensors and lack the motility apparatus. Motile cilia in primitive flagellated organisms and mammalian sperm flagella exist as a single axonemal structure. Additionally, a population of cells containing a single motile cilium is present within the embryonic node during somite development that is responsible for establishing left-right asymmetry (Nonaka et al., 1998). However, in epithelial cells of the airway, the oviduct, the choroid plexus and the ependymal cells, cilia are expressed as multiple axonemal structures. Recently, the forkhead transcription factor FoxJ1 has been shown to be necessary

[1]North Carolina State University, College of Veterinary Medicine, Department of Molecular Biomedical Sciences, Raleigh, NC 27606, USA. [2]North Carolina State University, College of Veterinary Medicine, Department of Population Health and Pathobiology, Raleigh, NC 27606, USA. [3]Division of Developmental Biology, Department of Pediatrics, Children's Hospital Medical Center, University of Cincinnati College of Medicine, Cincinnati, OH 45229, USA. [4]Cystic Fibrosis Research Center, University of North Carolina, Chapel Hill, NC 27599, USA. [5]Pulmonary and Critical Care Medicine, Department of Internal Medicine, Washington University School of Medicine, St Louis, MO 63110, USA.

*Author for correspondence (Troy_Ghashghaei@ncsu.edu)

Accepted 18 September 2009

and sufficient for the generation of motile cilia throughout the body in *Xenopus* and zebrafish (Yu et al., 2008; Stubbs et al., 2008). However, the role of FoxJ1 in the differentiation of ependymal cells and cellular organization in the SCN has remained unknown. Here we report the expression and function of FoxJ1 in the differentiation of the postnatal and adult SCN.

MATERIALS AND METHODS

Animals

Animals were used under Institutional Animal Care and Use Committee regulations and approval at North Carolina State University, and were housed at Laboratory Animal Research facilities at the College of Veterinary Medicine. *FoxJ1*^{EGFP} (Ostrowski et al., 2003), *FoxJ1*$^{-/-}$ (Brody et al., 2000) and *FoxJ1*$^{-/-EGFP}$ mice and their littermate controls were sacrificed at multiple developmental stages. For embryonic studies, the day of vaginal plug was considered embryonic day 0 (E0). For fixed analysis of tissue, animals were transcardially perfused with 4% paraformaldehyde in 0.1 M phosphate buffered saline (PBS), pH 7.4. Following perfusion, brains were removed and postfixed for a minimum of 24 hours.

For microarray experiments, mice at the multiple developmental time points were sex-genotyped by PCR amplification of the sex-determining region on the Y chromosome (*Sry*; forward primer, 5′-TGGGAC-TGGTGACAATTGTC-3′; reverse primer, 5′-GAGTACAGGTGTGC-AGCTCT-3′). RNA from male mice was extracted and processed for microarray analyses.

Tissue processing and immunohistochemistry

For immunohistochemistry, brains were sectioned at 50 μm on a vibratome (Leica VT 1000 S). E10 embryos and whole heads of postnatal day 0 (P0) newborn mice were fixed overnight, cryopreserved in 30% sucrose in PBS (containing 0.05% sodium azide), frozen in TissueTek at –80°C overnight and sectioned at 15-20 μm on a cryostat (Leica). Brain sections were blocked in 10% goat serum or 10% donkey serum (for experiments involving goat primary antibodies) with 1% Triton X-100 (Sigma, S26-36-23) in PBS, followed by incubation with primary antibodies at 4°C overnight. Appropriate goat or donkey secondary antibodies conjugated to Alexa 488, Cy3 and Alexa 647 were used for visualization (all diluted 1:1000, 1-hour incubation at room temperature). Primary antibodies used included: rabbit anti-Dlx2 (D. Eisenstat, University of Manitoba, Canada; 1:1000), mouse anti-FoxJ1 (1:200), mouse anti-Gfap (Milipore; 1:1000), rabbit anti-Gfap (Dakocytomation; 1:1000), chicken anti-GFP (Abcam; 1:2000), rabbit anti-Gsh2 (Gsx2 – Mouse Genome Informatics; K. Campbell; 1:4000), mouse anti-Lhx6 (Novus Biologicals; 1:200), rabbit anti-S100β (Sigma; 1:1000), rabbit anti-Blbp (Milipore; 1:500), mouse anti-RC1 (Cbx8 – Mouse Genome Informatics; Developmental Studies Hybridoma Bank University of Iowa; 1:250), mouse anti-BrdU (BD Bioscience; 13:1000), rabbit anti-Pax6 (Milipore; 1:500), mouse anti-Ncam (Abcam; 1:500), rat anti-CD31 (BD Pharmigen; 1:500), rat anti-CD133 (eBioscience; 1:1000), mouse anti-nestin (Chemicon; 1:1000), rabbit anti-β-catenin (Invitrogen; 1:500) and rabbit anti-γ-tubulin (Sigma; 1:1000). Some sections were counterstained with Alexa-647-conjugated Nissl stain (Invitrogen; 1:1000) for cytoarchitectonic assessment of labeled tissue.

For in situ hybridization, a probe corresponding to nucleotides 784-1368 of GenBank sequence NM_008240 (*FoxJ1*) was amplified by PCR from *FoxJ1* cDNA (ATCC, Manassas, VA, USA). Digoxigenin (DIG)-labeled antisense and sense riboprobes were generated using the DIG RNA Labeling Kit (Roche Diagnostics). Cryosections of adult brains were hybridized with riboprobes at 55°C for 30 hours. After washing and blocking, sections were incubated with anti-DIG antibody conjugated with alkaline phosphatase (1:1000) overnight at 4°C. DIG labeling was visualized using Nitro Blue Tetrazolium/5-bromo-4-chloro-3-indolyl phosphate development.

Intraventricular lentiviral and cell injections

Effective FoxJ1-specific shRNA sequences were identified (see Fig. S7 in the supplementary material). The *shFoxJ1*-lenti and control-lenti vectors were generated by transfecting viral constructs into human293 cells as described previously (Olsen, 1998; O'Rourke et al., 2005; Jacquet et al., 2009). EGFP reporter was expressed under the chicken β-actin promoter in both vectors for tracking transduction. For cell transplantation studies, *FoxJ1*$^{-/-EGFP}$ or *FoxJ1*$^{+/+EGFP}$ cells were injected into the lateral ventricles of wild-type and *FoxJ1*-null animals using a stereotaxic apparatus. Cell preparations were obtained using fluorescence-activated cell sorting (Dako Cytomation MoFlo; NCSU Flow Cytometry and Cell Sorting Laboratory), followed by resuspension in artificial cerebrospinal fluid (Ghashghaei et al., 2007b) supplemented with 10 ng of epidermal growth factor (Egf) and fibroblast growth factor (Fgf2) to a final concentration of 1×10^6 EGFP$^+$ cells/μl.

For both transplantation and lentiviral injections, newborn pups (P0) were anesthetized by means of hypothermia as described previously (Ghashghaei et al., 2007b). For *shFoxJ1*-lenti and control-lenti vector injections, 1 μl of each vector (10^{10} infectious units/ml) was injected into the anterior lateral ventricles of P0 pups using stereotaxic surgery (n=3 per construct). For cell transplantation studies, 1 μl of resuspended cells was injected into each hemisphere (10^6 EGFP$^+$ cells/μl). Wild-type pups were injected intraventricularly with control-lenti vector (n=3), *shFoxJ1*-lenti vector (n=3) or *FoxJ1*$^{-/-EGFP}$ cells (n=3). *FoxJ1*$^{-/-}$ pups were injected with *FoxJ1*$^{+/+EGFP}$ cells (n=3). Following surgery, injected pups were placed under a heating lamp to revive rapidly. The entire surgical procedure lasted less than 15 minutes for each pup. Pups were placed back with the dam 15-20 minutes after recovery and sacrificed at P21.

FoxJ1-independent hydrocephalic models

P0 wild-type B6/C57 mice were used for kaolin induction of hydrocephalus. Kaolin (Sigma, K1512-500G) was dissolved to a 25% working concentration in artificial cerebrospinal fluid as described previously (Ghashghaei et al., 2006). Pups were placed on ice for 1 minute to induce anesthesia by means of hypothermia and 3 μl of kaolin solution was injected into their cisterna magna over a period of less than 3 minutes. Injected pups were placed under a heating lamp until breathing stabilized over a 20-minute recovery period. Recovered pups were returned to their mother and those that developed hydrocephalus were sacrificed at P6 and P21 for analysis of differentiation in the SCN.

Dnaic1$^{-/-}$ mice (Ostrowski et al., 2009) were used as a genetic model for assessing the effects of hydrocephalus on SCN development and postnatal neurogenesis in the OB. The developmental time course of hydrocephalus in *Dnaic1*$^{-/-}$ mice was similar to that in *FoxJ1*$^{-/-}$ mice, starting between P1 and P6 with a progressive increase in ventricular volume by P21. *Dnaic1*$^{-/-}$ and wild-type littermates were perfused at P6 and P21 as described (n=3 per genotype for each age group). The brains were sectioned and assessed for SCN cell types as described above.

Neurosphere cultures

Brains from P0 and P21 *FoxJ1*$^{+/+EGFP}$ mice were rapidly collected, followed by microdissection and dissociation of the SVZ and RMS. Cells were sorted using a Dako Cytomation MoFlo and immediately cultured in Neurobasal medium supplemented with growth factors as described previously (Jacquet et al., 2009). The neurospheres obtained were passaged every 5 days by dissociation into individual cells followed by culturing in Neurobasal medium. After every passage, the percentage of EGFP$^+$ neurospheres was calculated by counting the number of neurospheres in each well (n=6 for each passage). Neurospheres were differentiated on laminin- and poly-L-lysine-coated chambered glass slides in Neurobasal medium without growth factors for 10 days. Differentiated cultures were fixed with 4% paraformaldehyde and immunostained as in tissue processing.

Data analysis

Tissue and cell culture analyses were performed using a confocal microscope (Nikon Eclipse C1) and data were quantified using standard stereological estimation methods as described previously (Ghashghaei et al., 2006). Significance was determined using Student's t-tests and all values were expressed as mean ± s.e.m.

Laser capture microscopy

Brains obtained from P1, P7 and P14 *FoxJ1*$^{+/+EGFP}$ male mice were collected in a 10% RNA preservation solution (50% ammonium sulfate, 10 mM EDTA, 25 mM sodium citrate in RNase-free water, pH=5.2) in PBS, embedded in RNase-free OCT medium and frozen at –80°C overnight.

Brains were then sectioned on a cryostat at 10 μm and collected on MembraneSlides (Zeiss; NF 1.0 PEN; 1 mm, nuclease and human nucleic acid free). The slides were UV-irradiated 30 minutes prior to use. Slides with sagittal *FoxJ1*$^{+/+EGFP}$ sections were rapidly placed under a Zeiss Axiovert 200 microscope coupled to a PALM microlaser system with epifluorescence capability. A 355 NANAO Laser was used for microdissection of *FoxJ1*$^{+/+EGFP}$ domains in the forebrain (laser spot size, 7.5 μm; pulse power, 100 mW; pulse duration, 0.8-1.5 milliseconds). Excised tissue was captured into Eppendorf tubes containing 10 μl of TRIzol (Invitrogen). The RNA was extracted by tissue homogenization in TRIzol, followed by RNA cleanup (Qiagen, Valencia, CA, USA).

Microarray experiments

Total RNA extracted from laser-captured *FoxJ1*^{EGFP} domains was used for microarray experiments. Expression profiling using Affymetrix GeneChip Mouse Gene 1.0 ST arrays was performed at the University of North Carolina Neuroscience Center, Functional Genomics Core Facility, including cRNA synthesis and Chip hybridization. Data obtained from *FoxJ1*$^{EGFP+}$ and *FoxJ1*$^{EGFP-}$ domains from wild-type and *FoxJ1*-null brains were compared at the three developmental time points, and those with an average fold-change of 1.5 or more (s.e.m. across three ages ≤0.1) were selected for subsequent analysis. Hierarchical clustering was performed on fold-changes calculated from normalized expression values on the $\log_2$ scale using MeV Multi Experimental Viewer software (version 4.1). A selection of genes encoding cytoskeleton-associated proteins with a statistically consistent fold-change across three postnatal developmental time points was confirmed by quantitative real-time PCR (qRT-PCR) as described below. Expression of the identified genes in the ependymal layer was confirmed in sections obtained from the Allen Brain Atlas at http://www.brain-map.org (see Fig. S9 in the supplementary material). The data discussed in this publication have been deposited in NCBI's Gene Expression Omnibus (Edgar et al., 2002) and are accessible through GEO Series accession number GSE18678.

Quantitative real-time PCR

Perinatal *FoxJ1* expression levels and the expression levels of selected genes encoding cytoskeleton-associated proteins were determined by qRT-PCR on independent samples (n=3 per age). PCR reactions were performed in duplicate using an iQ Cycler detection system (BioRad). The fold-change between paired samples was calculated using normalized data. cDNA was synthesized from RNA extracts according to the Taqman RT Kit protocol (ABI, Foster City, CA, USA). Primers were designed using Primer3 software (http://frodo.wi.mit.edu/primer3/input.htm). Primer sequences are provided in Table S2 in the supplementary material. Gene expression data were calculated using the $2^{-\Delta C_T}$ method (Livak and Schmittgen, 2001).

Reverse transcriptase (RT)-PCR

Total RNA was isolated using TRIzol extracts from whole brains, and the Protoscript II RT-PCR Kit (New England Biolabs) was used for cDNA preparation. PCR amplification was performed using gene-specific primers: 5′-GAGCTGGAACCACTCAAAGC-3′ and 5′-GGAACATGGGTGG-ATGAAAC-3′ for *FoxJ1*. Twenty-five cycles of amplification were performed by denaturing at 94°C for 30 seconds, annealing at 51°C for 30 seconds and elongation at 72°C for 2 minutes.

Co-immunoprecipitation and western blotting

Animals were euthanized by isofluorane overdose and brains from wild-type or *FoxJ1*$^{-/-}$ mice at various ages were rapidly collected and lysed for protein extraction. For detection of FoxJ1 protein levels, extracted proteins from E20 and P0 mice were transferred to a membrane and incubated with rabbit anti-FoxJ1 antibody (Affinity Bioreagents; 1:200) at 4°C overnight. For immunoprecipitation, lysates were incubated with primary antibodies against γ-tubulin (Sigma) at 4°C overnight. Immunoprecipitated proteins were then purified using Protein G-agarose beads according to the manufacturer's instructions (Invitrogen). Samples were run on a reducing SDS-PAGE gel followed by semi-dry transfer to a nitrocellulose membrane. The membrane was then blocked (5% skimmed milk powder), exposed to primary antibodies against Dnaic (Milipore), Dnahc (Santa Cruz) and Kif6 (AbCam). Membranes were incubated with the appropriate secondary antibodies (goat anti-rabbit or anti-mouse) conjugated to horseradish peroxidase (Millipore; 1:1000) at room temperature for 1 hour. All membranes were developed for visualizing labeled bands with an ECL Kit (Pierce, 32106).

RESULTS

The forkhead transcription factor FoxJ1 is expressed in the adult SCN

Examination of adult mice expressing enhanced GFP regulated by the *FoxJ1* promoter (*FoxJ1*^{EGFP}) (Ostrowski et al., 2003) indicated high levels of FoxJ1 expression in the ventricular epithelium and the hippocampal dentate gyrus (Fig. 1A; see Fig. S1 in the supplementary material). In situ hybridization and immunohistochemistry confirmed the validity of transgene expression in the SVZ (Fig. 1B,C). High-magnification marker analysis revealed that most ependymal cells positive for the calcium binding protein S100β express FoxJ1 in the SVZ (Fig. 1D). Subsets of FoxJ1$^+$ cells in contact with the ventricles co-expressed the surface protein CD133 (Prominin 1 – Mouse Genome Informatics), which has recently been shown to label ependymal cells in the adult SVZ (Fig. 1E) (Coskun et al., 2008). In addition, an intriguing subset of astrocytes in the SVZ, positive for the glial fibrillary acidic protein (Gfap), expressed FoxJ1 (Fig. 1F,G). By contrast, FoxJ1 was largely absent in TAPs positive for the epidermal growth factor receptor (Egfr; Fig. 1H). Most FoxJ1$^+$ astrocytes had an elongated process that contacted CD31$^+$ (Pecam 1 – Mouse Genome Informatics) blood vessels within the SVZ (Fig. 1I) (Tavazoie et al., 2008).

In the RMS, migrating neuroblasts expressing the polysialylated neuronal cell adhesion molecule (PSA-NCAM), Gfap$^+$ astrocytes and S100β$^+$ glia (not shown) lacked *FoxJ1*^{EGFP} expression (Fig. 1J-K). However, most *FoxJ1*^{EGFP} cells in the RMS were positive for the immature radial glia markers brain lipid-binding protein (Blbp) and nestin (Fig. 1L). A few cells also expressed low levels of the paired homeobox domain transcription factor Pax6 (Fig. 1L). Thus, *FoxJ1*^{EGFP} cells may constitute a distinct progenitor population in the RMS.

In the OB, a large proportion of *FoxJ1*^{EGFP} cells were Gfap$^+$ astrocytes, but neurons were devoid of *FoxJ1*^{EGFP} expression (Fig. 1M,N). Taken together, this cellular characterization indicates that FoxJ1 is primarily expressed by ependymal cells and a small subset of astrocytes in the SVZ. We also found that *FoxJ1*^{EGFP} cells in the RMS constitute a potential population of Blbp$^+$ nestin$^+$ Pax6$^+$ progenitors, whereas most *FoxJ1*^{EGFP} cells in the OB are a subset of astrocytes.

Ependymal cells and FoxJ1$^+$ astrocytes appear in the SVZ during two distinct postnatal time-points

Based on cell- and region-specific localization of FoxJ1 in the brain, we next mapped *FoxJ1*^{EGFP} expression prior to birth. *FoxJ1*^{EGFP} expression in the rostral forebrain included the choroid plexus, as well as the radial glial cells on and near the ventricular surface of the lateral ganglionic eminence (LGE) and the olfactory ventricles (Fig. 2A; see Fig. S2 in the supplementary material). Perinatal mapping and quantification revealed that FoxJ1 was significantly upregulated at birth (P0), compared with just before birth (E20; Fig. 2A-E). At P1, the density of *FoxJ1*^{EGFP} cells increased along the walls of the ventricles throughout the brain, where the new cells were cuboidal in morphology rather than elongated, similar to *FoxJ1*$^{EGFP+}$ radial glial cells in the LGE (Fig. 2F,F′). By P6, many of the expanding FoxJ1$^+$ cells began to express S100β and clearly resembled ependymal cells (Fig. 2G,H), matching the timing of ependymal cell maturation reported previously (Spassky et al., 2005). Notably, the

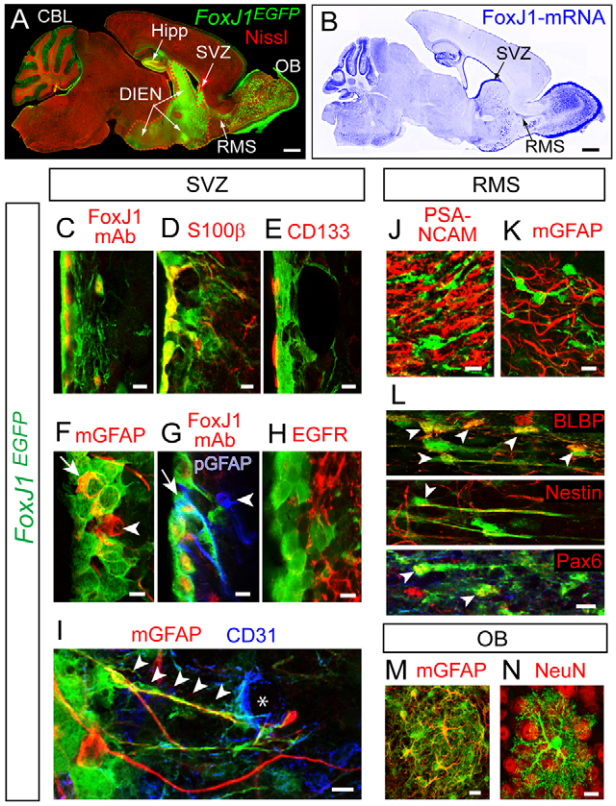

Fig. 1. FoxJ1 expression in the adult brain. (**A**) Nissl (red) stained sagittal section of an 8-week-old adult *FoxJ1*^{EGFP} mouse brain reveals EGFP expression in the hippocampus (Hipp), cerebellum (CBL), a subset of diencephalic nuclei (DIEN), SVZ, RMS and OB. (**B**,**C**) In situ hybridization (B, blue) and immunostaining using a monoclonal FoxJ1 antibody (FoxJ1-mAb; C, red) confirmed transgene expression in the SVZ, RMS and OB. (**D-N**) High-magnification confocal micrographs of *FoxJ1*^{EGFP}-expressing cell types in the SVZ (D-I), RMS (J-L) and OB (M,N). A small subset of cells positive with a monoclonal FoxJ1 antibody and for *FoxJ1*^{EGFP}, co-labeled with a polyclonal Gfap antibody (G, pGfap, blue; arrow, a triple-labeled FoxJ1$^+$ astrocyte; arrowhead, a FoxJ1$^-$ astrocyte). Many FoxJ1$^+$ astrocytes in the SVZ have an elongated process (I, arrowheads) that contacts blood vessels positive for CD31 (I, asterisk, blue). In the RMS, many *FoxJ1*^{EGFP} cells express the immature/radial glial marker brain lipid binding protein (Blbp; L, arrowheads). A few also express the progenitor-specific intermediate filament nestin and the paired homeobox domain transcription factor Pax6 (L, arrowheads). Scale bars: 100 μm in A,B; 10 μm in C-N.

emergence of S100β$^+$ ependymal cells was delayed in regions with embryonic *FoxJ1*^{EGFP} expression (e.g. the ventricular zone of the LGE). Accordingly, ependymal cells appeared to differentiate earlier (between P1 and P6) in non-striatal regions of the ventricular zone, such as the ventricular zone of the septum and the dorsal ventricular surface underneath the corpus callosum.

Intriguingly, a subset of FoxJ1$^+$ Blbp$^+$ radial glia found in the LGE (see Fig. S2 in the supplementary material) persisted in the SVZ at P6, and were anatomically distinct from maturing FoxJ1$^+$ and S100β$^+$ cells. FoxJ1$^+$ Blbp$^+$ cells were predominantly situated in the TAP layer (Fig. 2G,I) and RMS (Fig. 2J), and only a few were intercalated among ependymal cells. Therefore, by P6, an initial wave of differentiation in FoxJ1$^+$ cells was specific to the maturation of ependymal cells. However, we could not detect any FoxJ1$^+$ astrocytes in the SVZ at this stage, but found a subset of radial glia that appear to persist in the SVZ and RMS during early postnatal development.

To time the emergence of FoxJ1$^+$ astrocytes found in the adult SCN (Fig. 1F,G,I), we labeled for S100β as a marker for ependymal cells, and used a monoclonal antibody against Gfap (mGfap) for SVZ astrocytes. The majority of FoxJ1$^+$ cells prior to P19 were nascent S100β$^+$ mGfap$^-$ ependymal cells and Blbp$^+$ mGfap$^-$ radial glial-like cells (Fig. 2K). Interestingly, between P19 and P21, a subset of FoxJ1$^+$ cells intercalated between ependymal cells began to express mGfap (Fig. 2K). These FoxJ1$^+$ S100β$^-$ mGfap$^+$ cells became more abundant between 6 weeks (1.6±0.5% of all astrocytes in the SVZ) and 6 months (2.1±0.6% of all astrocytes in the SVZ) postnatal (n=3 per age group; Fig. 2L). Thus, after the significant upregulation of FoxJ1 in the forebrain after birth, FoxJ1$^+$ ependymal cells differentiate during the first postnatal week. This is followed by a second wave of differentiation during the end of the third postnatal week, when a small subset of FoxJ1$^+$ SVZ astrocytes begin to differentiate and their density gradually increases for the first 6 months of life.

FoxJ1 is required for postnatal differentiation of ependymal cells and FoxJ1$^+$ astrocytes in the SVZ

Changes in temporal and spatial expression of FoxJ1 in the brain inspired the hypothesis that the two postnatal waves of differentiation in FoxJ1$^+$ cells are required for SCN maturation during the LGE-to-SVZ transition. To test this hypothesis, we used *FoxJ1* knockout mice (*FoxJ1*$^{-/-}$), which exhibit random asymmetry defects associated with the absence of motile cilia throughout development (Brody et al., 2000). *FoxJ1*$^{-/-}$ mice that do not exhibit aberrant left/right asymmetry survive into early adulthood, but the surface of their cerebral ventricles is devoid of motile cilia and they develop hydrocephalus (Fig. 3A-D′). Importantly, growth defects were quantified in multiple brain regions at P21, and those in the *FoxJ1*$^{-/-}$ OB were most significant (66±12% reduction in volume; Fig. 3A-B′; see Fig. S3 in the supplementary material).

Retarded growth in the *FoxJ1*$^{-/-}$ mouse OB, together with the restricted expression of *FoxJ1*^{EGFP} in the LGE and olfactory ventricles, suggested a possible alteration of specification events in these structures, whereby OB neurogenesis occurs during embryonic and perinatal periods (Hinds, 1968a; Hinds, 1968b; Bayer, 1983; Gong and Shipley, 1995). Surprisingly, we only found subtle changes in the patterning, density and proliferation of known progenitor domains in the LGE and in the olfactory ventricular zone prior to birth (see Fig. S4 in the supplementary material), and embryos and newborn *FoxJ1*$^{-/-}$ animals appeared grossly normal in size and in brain organization. Additionally, primary cilia were expressed, in a similar manner to in wild-type animals, on the apical surface of radial glia lining the ventricular zone of the embryonic *FoxJ1*$^{-/-}$ LGE, suggesting that FoxJ1 is not required for genesis of primary cilia (see Fig. S4 in the supplementary material). These findings, together with the marked upregulation of FoxJ1 at birth, prompted us to hypothesize that FoxJ1 expression could have a temporally focused role in postnatal establishment of the SCN. To examine this possibility, we first asked whether constituents of the postnatal SCN were appropriately specified in the P6 *FoxJ1*$^{-/-}$ SVZ using S100β labeling. Indeed, we found that S100β$^+$ cuboidal cells failed to emerge in the ventricular wall of P6 *FoxJ1*$^{-/-}$ mice (see Fig. S5 in the supplementary material), suggesting that FoxJ1 is required for ependymal cell differentiation.

To determine whether a mature adult SCN ever develops in *FoxJ1*$^{-/-}$ mice, cellular integrity of astrocytes and ependymal cells was examined at P21, at which time the adult-stage SCN is

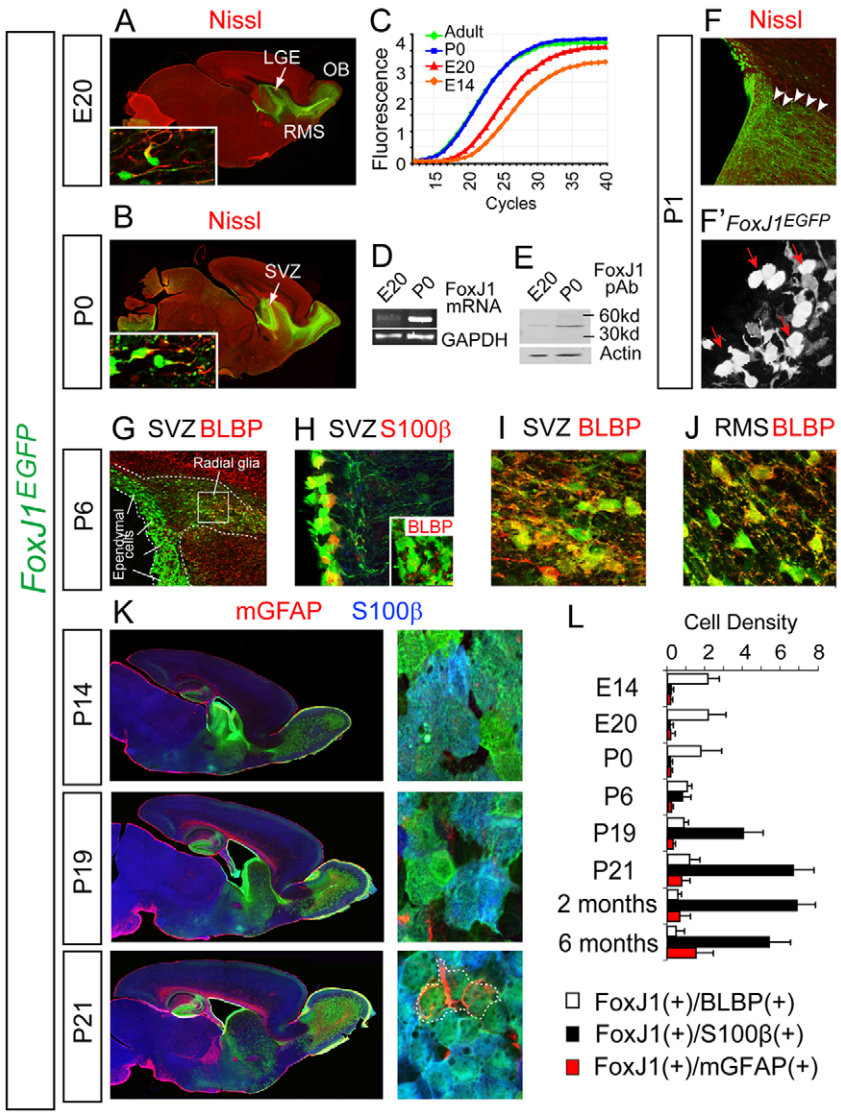

Fig. 2. Emergence of FoxJ1⁺ cells in the postnatal SCN. (**A-E**) *FoxJ1*^{EGFP} expression in the E20 mouse embryo is present in nestin⁺ cells with radial glial morphology (A, inset) on the walls of the lateral ganglionic eminence (LGE), the olfactory ventricle (RMS) and the OB. In the SVZ, transforming *FoxJ1*$^{EGFP+}$ nestin⁺ radial glia (B, inset) begin to lose their uniform polarized processes. Upregulation of FoxJ1 at birth was quantified by real-time PCR (C), reverse transcriptase (RT)-PCR (D) and western blotting (E). (**F**,**F′**) At P1, FoxJ1⁺ radial glia persist deep in the SVZ and RMS (F, arrowheads), while ependymal cells start to appear in the SVZ adjacent to the ventricular lumen (F′, cuboidal cells, red arrows). (**G-J**) At P6, the ependymal layer expands (G) and *FoxJ1*$^{EGFP+}$ S100β⁺ cells become pronounced (H). Dashed lines demarcate the SVZ in G. Ependymal cells do not express the radial glial marker Blbp (H, inset). A distinct population of *FoxJ1*$^{EGFP+}$ Blbp⁺ cells persist in the deep regions of the SVZ (boxed area labeled radial glia in G is magnified in I) and in the RMS (J). (**K**) Low-magnification micrographs of sagittal sections from P14, P19 and P21 *FoxJ1*^{EGFP} brains stained for mGfap (red) and S100β (blue). High-magnification panels are confocal micrographs of a flat embedded ependymal layer prepared from the corresponding sagittal sections. Arrival of the newly discovered FoxJ1⁺ astrocytes (outlined by the dotted line) occurs between P19 and P21. (**L**) The density of distinct types of FoxJ1⁺ cells at multiple postnatal time points. The data in L are stereological estimates obtained from triple-labeled tissues (cell density = number of cells × 10^4/mm^3, n=3 per age group).

established. Transmission and scanning electron microscopy clearly demonstrated the absence of motile cilia on the surface of the *FoxJ1*$^{-/-}$ SVZ, as well as the disrupted organization of the ependymal layer in these mice (Fig. 3C-D′). Despite the absence of motile cilia, primary cilia were present in the *FoxJ1*$^{-/-}$ SVZ (see Fig. S6 in the supplementary material). As suspected, S100β⁺ mGfap⁻ ependymal cells were almost absent (Fig. 3E,E′) and CD133 expression was substantially decreased in the *FoxJ1*$^{-/-}$ SVZ (Fig. 3F,F′). These findings demonstrated that in the absence of FoxJ1 expression, ependymal cells fail to mature at any developmental stage. In their place, we found a significant number of residual immature Blbp⁺ cells (Fig. 3G,G′), suggesting that subsets of *FoxJ1*$^{-/-}$ radial glia may be arrested in an undifferentiated state.

FoxJ1 is cell-autonomously required for differentiation of the SCN

Based on the perturbed cell-specific phenotypes, we set out to clearly assess the autonomous and non-autonomous effects of *FoxJ1* deletion on the cellular constituents of the adult SCN. To accomplish this, we crossed our *FoxJ1*^{EGFP} reporter mice into the *FoxJ1*$^{-/-}$ background to obtain *FoxJ1*$^{-/-EGFP}$ animals. The overall density of *FoxJ1*$^{-/-EGFP}$ cells was higher than in *FoxJ1*$^{+/+EGFP}$ controls in the SVZ, and they were significantly smaller than wild-type cells (Fig. 4A). As suspected, nearly all *FoxJ1*$^{-/-EGFP}$ cells expressed Blbp, suggesting that they had failed to mature (Fig. 4B). Additionally, the *FoxJ1*$^{-/-}$ SVZ included a significant increase in density of mGfap⁺ cells resembling reactive astrocytes, with densely distributed processes adjacent to *FoxJ1*$^{-/-EGFP}$ cells (Fig. 4B, asterisks). However, a significantly smaller percentage of *FoxJ1*$^{-/-EGFP}$ cells in the SVZ were Gfap⁺ compared with those in *FoxJ1*$^{+/+EGFP}$ mice (9±0.3% vs 19±0.8%, respectively; Fig. 4B). Thus, FoxJ1 is, in part, required for differentiation of FoxJ1⁺ astrocytes that emerge by P21 in the wild-type SVZ.

Next, to examine the rosette/pinwheel architecture of ependymal and astrocytic cells on the surface of the lateral ventricles, we obtained wholemount preparations of the ependymal layer and immunostained for Gfap together with β-catenin and γ-tubulin (Fig. 4C). β-catenin, an important constituent of the Wnt signaling pathway (Schlessinger et al., 2009), is expressed on the lateral and apical surfaces of wild-type ependymal cells. γ-tubulin is a component of a microtubule-organizing complex at the base of individual cilia and is crucial for their growth and maintenance (Oakley, 1992) and clearly decorates the apical surface of multiciliated ependymal cells (Mirzadeh et al., 2008). The rosette/pinwheel organization of ependymal cells and astrocytes was

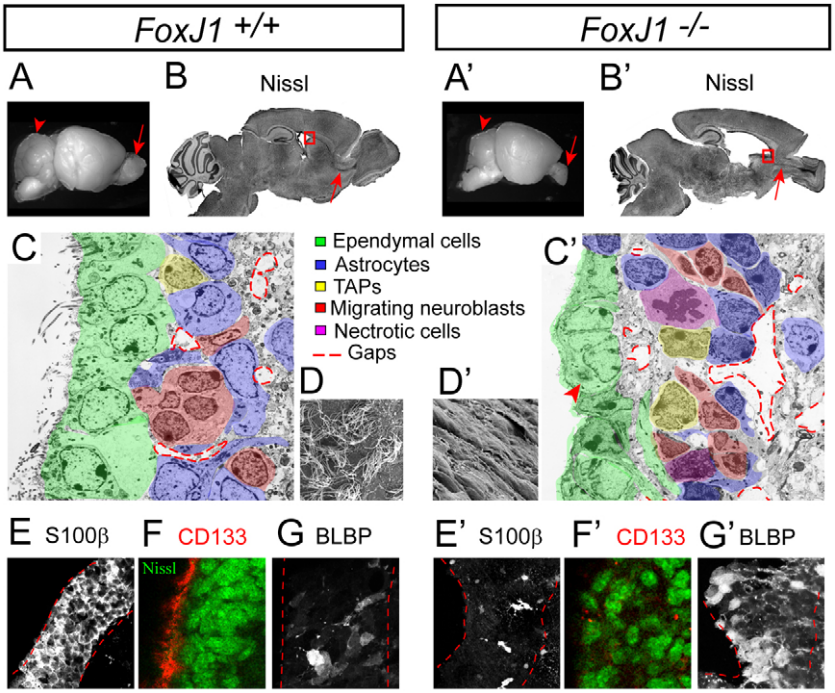

Fig. 3. *FoxJ1*$^{-/-}$ mice fail to establish the SCN. (**A**,**A**′) Photomicrographs of P21 brains harvested from wild-type (A) and *FoxJ1*$^{-/-}$ (A′) littermates. Arrows point to the OB and arrowheads to the cerebellum. (**B**,**B′**) Sagittal sections of P21 brains harvested from wild-type and *FoxJ1*$^{-/-}$ littermates. Arrows point to the RMS, boxed areas demarcate regions shown in high-magnification confocal images in E-G′. (**C**,**C′**) Transmission electron micrographs obtained from the ventricular zone of P21 wild-type (C) and *FoxJ1*$^{-/-}$ (C′) littermates. Colored cells were classified based on description by a previous study (Doetsch et al., 1997). The red arrowhead points to unusual aggregates within *FoxJ1*$^{-/-}$ undifferentiated ependymal cells. (**D**,**D′**) Scanning electron micrographs obtained from the ventricular surface of the SVZ show a complete lack of cilia in *FoxJ1*$^{-/-}$ mice but their clear presence in wild-type animals. (**E-F′**) S100β^{+} and CD133^{+} ependymal cells in wild-type mice and their absence in *FoxJ1*$^{-/-}$ SVZs. (**G**,**G′**) Residual Blbp^{+} radial glia are in the position of the ependymal cells in the *FoxJ1*$^{-/-}$ SVZ.

absent on the surface of *FoxJ1*$^{-/-}$ ventricles, concomitant with a disruption of junctional β-catenin expression (Fig. 4C). To determine whether or not disrupted junctional β-catenin expression was due to the loss of junctional complexes in the *FoxJ1*$^{-/-}$ SVZ, we conducted transmission electron microscopy (TEM) analyses. Junctional complexes along the walls of mutant cells were readily detectable, although their orientation and positioning were severely disrupted (see Fig. S6 in the supplementary material). Thus, disrupted β-catenin expression in the *FoxJ1*$^{-/-}$ SVZ is not due to a complete loss of junctional complexes within mutant cells along the ventricles.

FoxJ1$^{-/-EGFP}$ cells included unusually large aggregates of γ-tubulin within their cytoplasm (Fig. 4C, arrowheads), suggesting that, in the absence of FoxJ1 expression, γ-tubulin fails to be distributed and docked at the apical surface of differentiating ependymal cells. TEM analysis of the P21 SCN revealed the presence of multiple basal bodies within *FoxJ1*$^{-/-}$ cells lining the ventricles (Fig. 4D). This suggests that the aggregates of γ-tubulin-immunoreactive particles are likely to correspond to basal bodies within the cytoplasm of *FoxJ1*$^{-/-}$ cells. To determine whether the aggregation of basal bodies was developmentally related to their replication during early postnatal ciliogenesis, we conducted TEM analysis of the P6 SVZ. We found that structures containing basal bodies, referred to as deuterosomes (Spassky et al., 2005), were visible within differentiating wild-type ependymal cells, but could not be found in the *FoxJ1*$^{-/-}$ cells lining the ventricles (Fig. 4D). Instead, aggregates of unorganized basal bodies were found within the cytoplasm of P6 *FoxJ1*$^{-/-}$ cells, suggesting that the formation of deuterosomes, and possibly the transport of basal bodies, was disrupted in the absence of FoxJ1 expression.

To rule out potential bystander effects from whole-body knockout of FoxJ1, we cloned and tested a short hairpin RNA (shRNA) sequence for acute knockdown of FoxJ1 expression (see Fig. S7 in the supplementary material). We found identical phenotypes to those in *FoxJ1*$^{-/-EGFP}$ cells, suggesting a cell-autonomous role for FoxJ1 in the differentiation of the SCN (see Fig. S7 in the supplementary material).

Finally, to confirm whether FoxJ1 functions cell-autonomously, and whether the wild-type or knockout environments influenced the observed phenotypes, we performed transplantation studies in newborn mice. P0 *FoxJ1*$^{+/+EGFP}$ and *FoxJ1*$^{-/-EGFP}$ cells were cross-transplanted into P0 wild-type and knockout mice without EGFP reporter expression, and host mice were allowed to survive to P21 (Fig. 5A). We found that wild-type EGFP^{+} cells transplanted into *FoxJ1*$^{-/-}$ ventricles incorporated into the host SVZ and differentiated into multiciliated ependymal cells despite their *FoxJ1*$^{-/-}$ environment (Fig. 5B,C). *FoxJ1*$^{-/-EGFP}$ cells injected into wild-type ventricles also incorporated into the wild-type ependymal layer, but failed to mature into multiciliated ependymal cells (S100β; arrows) or astrocytes (mGfap; asterisks) and maintained a Blbp^{+} identity (n=3; Fig. 5B,D). Concomitantly, CD133^{+} cilia were present in more than 80±16% of *FoxJ1*$^{+/+EGFP}$ cells transplanted into knockout host brains (n=3), whereas there was no apparent CD133 expression by *FoxJ1*$^{-/-EGFP}$ cells transplanted into wild-type host brains (Fig. 5B,D). As in other experiments, aggregates of γ-tubulin were consistently found in the transplanted *FoxJ1*$^{-/-EGFP}$ cells, whereas adjacent EGFP^{-} wild-type ependymal cells included speckles of γ-tubulin on their apical surface (Fig. 5C, arrowheads). In summary, results from knockout, shRNA and cross-transplantation experiments conclusively show that FoxJ1 is required for the differentiation of ependymal cells and a subset of FoxJ1^{+} astrocytes in the ventricular zone of the brain in a cell-autonomous manner.

FoxJ1$^{-/-}$ phenotypes are independent of hydrocephalus

A possible cause of defects in the P21 *FoxJ1*$^{-/-}$ ventricular zone might be due to the presence of hydrocephalus. We explored this issue by examining ependymal cell and astrocytic integrity in two independent models of hydrocephalus, one genetic and the other obstructive. First, genetic deletion of a major component of the axonemal dyneins in motile cilia [axonemal intermediate chain 1 (*Dnaic1*)] resulted in altered cilia motility and subsequent non-obstructive hydrocephalus (*Dnaic1*$^{-/-}$; see Fig. S8 in the supplementary material). The initiation and progression of hydrocephalus in these mice is similar to that in

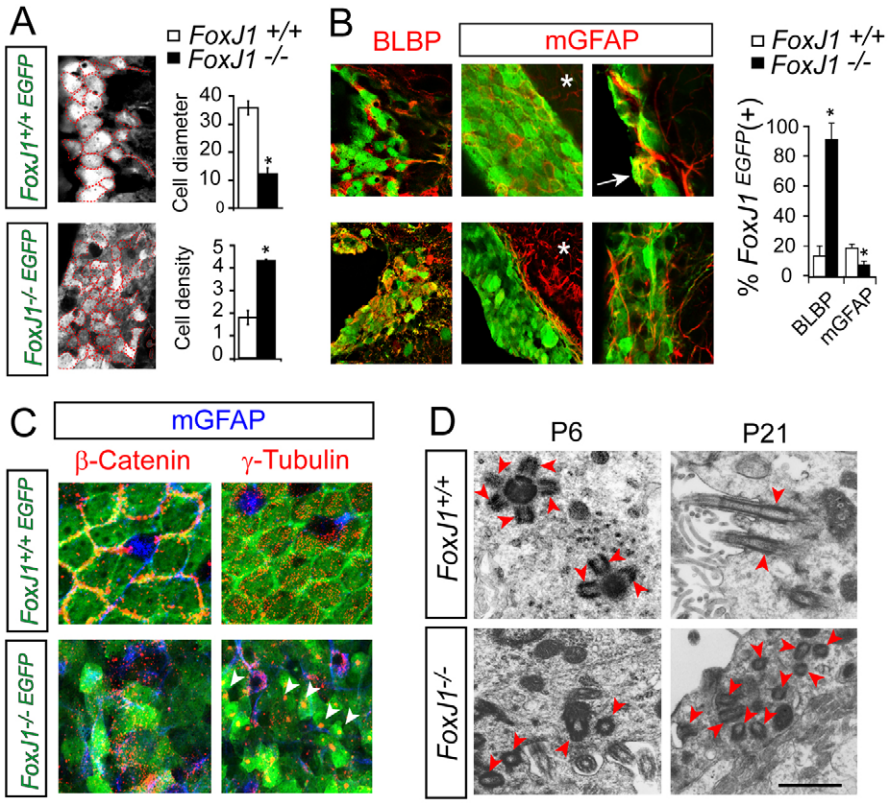

Fig. 4. Disrupted cellular differentiation in the *FoxJ1*$^{-/-}$ SVZ. (**A**) Confocal photomicrographs from the surface of the ventricles in the SVZs of *FoxJ1*$^{+/+EGFP}$ and *FoxJ1*$^{-/-EGFP}$ mice. *FoxJ* $^{-/-EGFP}$ cells were traced in the SVZ (red dotted lines). Cell density was estimated using stereological cell counting (number of cells × 10^4/mm^3). Cell diameter was defined as the longest distance between two ends of each cell and is presented in μm (33 cells in three individuals per genotype; mean ± s.e.m.; asterisk, P<0.01, Student's t-test). (**B**) *FoxJ1*$^{+/+EGFP}$ and *FoxJ1*$^{-/-EGFP}$ mice were assessed for expression of Blbp and mGfap on the surface of the SVZ. Reactive astrogliosis in the *FoxJ1*$^{-/-EGFP}$ SVZ did not overlap with the EGFP$^+$ domain containing *FoxJ1*$^{-/-}$ cells, but was deep within the adjacent TAP domain and striatal tissue (asterisks). mGfap panel to the right shows overlap of *FoxJ1*$^{+/+EGFP}$ and *FoxJ1*$^{-/-EGFP}$ cells in the P21 SVZ with mGfap$^+$ astrocytes at high-magnification (arrow). The bar chart illustrates the percentage of *FoxJ1*$^{+/+EGFP}$ and *FoxJ1*$^{-/-EGFP}$ cells positive for Blbp and mGfap (3 mice per genotype; n=50 cells per mouse). (**C**) *FoxJ1*$^{-/-EGFP}$ ventricles completely lack the rosette/pinwheel organization and β-catenin and γ-tubulin expression is massively disrupted. Large aggregates of γ-tubulin are found within *FoxJ1*$^{-/-}$ cells (arrowheads). (**D**) TEM images of basal body (red arrowheads) organization in the *FoxJ1*$^{+/+}$ and *FoxJ1*$^{-/-}$ SVZ. At P6, deuterosomes found in the wild-type SVZ cannot be detected in *FoxJ1*-null mice (red arrowheads). By P21, basal bodies have been successfully transported to, and docked at, the apical surface of wild-type ependymal cells, whereas in *FoxJ1*$^{-/-}$ cells only aggregates of basal bodies can be found in an unorganized manner. Scale bar: 1 μm.

FoxJ1$^{-/-}$ mice. In another model, injection of kaolin (Marlin et al., 1978) into the cerebra magna of P0 wild-type mice resulted in significant hydrocephalus by P6. The SCNs of *Dnaic1*$^{-/-}$ and kaolin-injected mice were analyzed at P6 and P21. In contrast to an absence of S100β$^+$ ependymal cells in *FoxJ1*$^{-/-}$ mice, this population was clearly present and aligned along the ventricular surface of both hydrocephalus models (see Fig. S8 in the supplementary material). However, both models displayed varying degrees of reactive astrogliosis at P21, which was also present on the ventricular surface of *FoxJ1*$^{-/-}$ mice and has been reported in other mice with hydrocephalus (Kuo et al., 2006). Thus, the absence of ependymal cells and disrupted differentiation in a subset of astrocytes in the *FoxJ1*$^{-/-}$ SVZ appears to be independent of increased intraventricular pressure due to hydrocephalus.

Developmental potential of *FoxJ1*^{EGFP} cells in the SCN

Our discovery of a small subset of FoxJ1$^+$ astrocytes in the SCN raised the question of whether they possess properties of neural stem cells. To address this, cells were dissociated from microdissected SVZs of P0 and P21 *FoxJ1*^{EGFP} mice. EGFP$^+$ and EGFP$^-$ cells were FACS sorted and cultured in the presence of growth factors for several days (Fig. 6A,B). Both populations gave rise to neurospheres, which are clones of neural stem cells (Reynolds and Weiss, 1992). Interestingly, cells within EGFP$^-$ neurospheres began to express *FoxJ1*^{EGFP} after 1 week (Fig. 6B, red arrows), suggesting either transformation or differentiation into FoxJ1$^+$ cells from the EGFP$^-$ pool of neurosphere progenitors during the in vitro culture period. The number and size of neurospheres were similar between EGFP$^+$ and EGFP$^-$ groups, and both groups could be passaged at least ten times, suggesting that *FoxJ1*^{EGFP} cells possess self-renewal capacity (Fig. 6C). Both groups of neurospheres were then plated onto laminin and poly-L-lysine for 10 days and their progeny differentiated into astrocytes, oligodendrocytes and neurons (Fig. 6D). The preferential shift toward gliogenesis was noted in both EGFP$^+$- and EGFP$^-$-derived neurospheres, but many neurons were also found within cultures. This finding suggests that a subpopulation of *FoxJ1*^{EGFP} cells possesses self-renewal and neurogenic potential in vitro, and these cells may function as stem cells in the adult SCN.

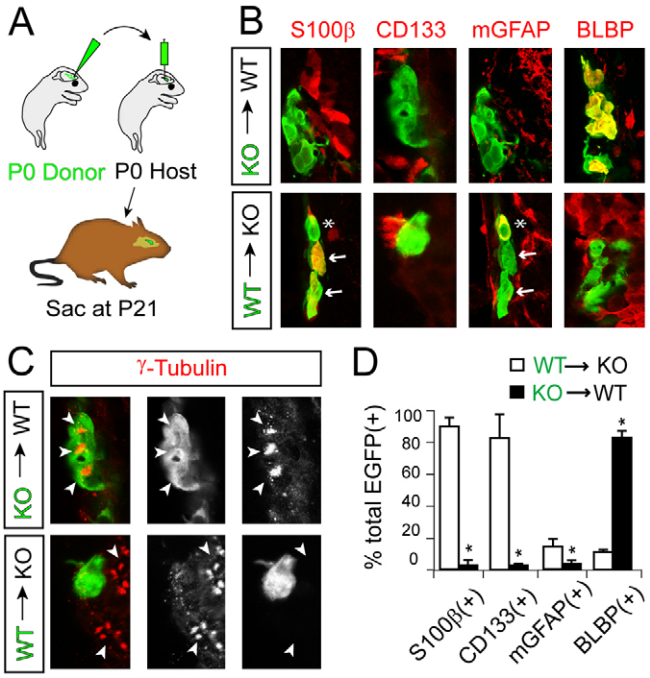

Fig. 5. FoxJ1 is cell-autonomously required for ependymal and astrocytic cell differentiation. (**A**) Cross-transplantation of *FoxJ1*$^{-/-EGFP}$ knockout (KO) and *FoxJ1*$^{+/+EGFP}$ wild-type cells into EGFP$^-$ wild-type and *FoxJ1* $^{-/-}$ KO hosts. (**B**) Wild-type cells differentiate into ependymal cells (arrows, S100β$^+$; CD133$^+$) and a subset of astrocytes (asterisks, Gfap$^+$) despite their KO host environment. KO cells remain immature (Blbp$^+$), despite their wild-type host environment. (**C**) Aggregates of γ-tubulin are present in KO cells or within the EGFP$^-$ KO host SVZ (arrowheads). (**D**) The percentage of EGFP$^+$ cells expressing different markers in the SCN (n=3 mice per genotype, 50 EGFP$^+$ cells per mouse). Data are mean ± s.e.m.; asterisks, P<0.01, Student's t-test.

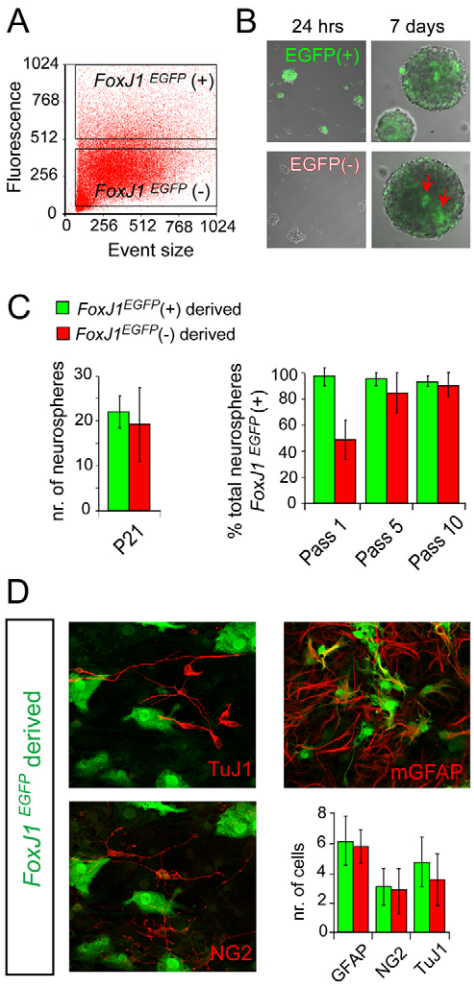

Fig. 6. Differentiation potential of *Fox*^{EGFP} cells in the postnatal SCN. (**A**,**B**) P21 SCN-derived *FoxJ1*^{EGFP} cells were FACS-sorted (A) and cultured to form neurospheres (B). *FoxJ1* promoter activity was maintained in floating neurospheres derived from EGFP$^+$ fractions and became visible in some EGFP$^-$-derived neurospheres (arrows) after 7 days of growth in vitro. (**C**) *FoxJ1*$^{EGFP+}$ and *FoxJ1*$^{EGFP-}$ neurospheres generated similar numbers of neurospheres at P21. The percentage of neurospheres that included *FoxJ1*$^{EGFP+}$ cells gradually increased in EGFP$^-$-derived cells, suggesting that at least a subset of *FoxJ1*^{EGFP} cells from the SCN can self-renew. The numbers of neurospheres are per 10 mm^2 culture wells. (**D**) *FoxJ1*^{EGFP}-derived neurospheres gave rise to neurons (TuJ1$^+$), astrocytes (mGfap$^+$) and oligodendrocytes (NG2$^+$) after 10 days of differentiation on laminin and poly-L-lysine. A subset of *FoxJ1*^{EGFP} cells persisted in differentiated cultures (green cells). The numbers of cells in the bar chart are per 10^5 μm^2.

Identification of target genes influenced by FoxJ1 expression

The role of FoxJ1 in differentiation of the postnatal SCN naturally leads to the question of how FoxJ1 carries out its developmental functions. To identify candidate genes in the brain regulated by FoxJ1, we compared the expression of genes in *FoxJ1*$^{+/+EGFP}$ and *FoxJ1*$^{-/-EGFP}$ domains of the forebrain during the span of adult SCN development (P1, P7, P14) using laser capture micro-dissection (Fig. 7A) and microarray transcriptome analysis. This analysis revealed that 198 genes were altered more than 1.5-fold in a consistent manner at P1, P7 and P14. We used a stringent statistical criterion to only include genes with an s.e.m. of less than or equal to 0.1 of the average fold-change of their expression across the three ages (<10% error). Of the identified genes, 197 were consistently downregulated in *FoxJ1*$^{-/-EGFP}$ domains, whereas only one gene that met the statistical criterion above was consistently upregulated at P1, P7 and P14.

We next asked which of the identified genes had known cellular or molecular functions and were expressed in the ependymal zone of the adult brain using the Allen Brain Atlas. This analysis narrowed the list to 55 genes with known functions and ependymal zone expression, all of which were consistently downregulated in the *FoxJ1*$^{-/-EGFP}$ brain (see Table S1 in the supplementary material). Remarkably, of the 55 known downregulated genes, 24 encoded cytoskeleton-associated molecular motors, and sperm/flagellar-associated proteins (43% of identified genes encoded proteins with known functions). Sixteen of the 24 genes encode microtubule-associated proteins, including six distinct isoforms of dynein axonemal heavy chain, and three dynein intermediate chain-like proteins (Fig. 7B). Additionally, genes for three members of the kinesin family of motor proteins (Kif6/9/27) were significantly and consistently downregulated in the *FoxJ1*$^{-/-}$ SCN. The list also included a radial spokehead-like gene (*Rshl3*), a gene encoding the microtubule-associated protein Tekt4, and another for tubulin-tyrosine ligase-like family member 6 (*Ttll6*). To test the validity of microarray data, changes in expression of genes encoding microtubule-associated proteins were confirmed by qRT-PCR on three independent samples from *FoxJ1*$^{-/-}$ and wild-type brains at P1, P7 and P14 (Fig. 7B).

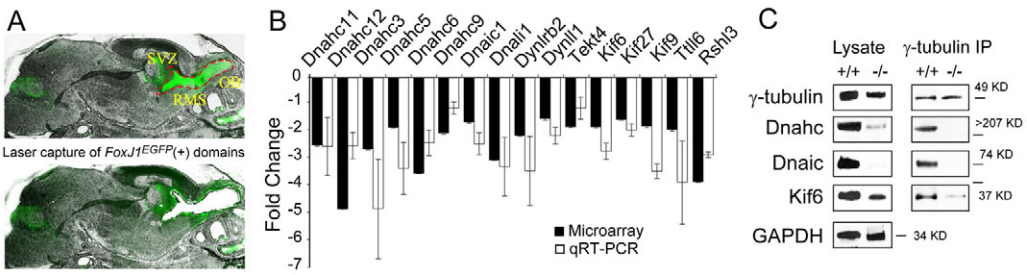

Fig. 7. Identification of candidate genes regulated by FoxJ1 during postnatal maturation of the SCN. (**A**) *FoxJ1*^{EGFP} domains in the rostral forebrain were laser-capture microdissected and processed for microarray analysis. (**B**) Comparison of wild-type and *FoxJ1*$^{-/-}$ array data resulted in the identification of 16 genes encoding microtubule-associated proteins that are significantly downregulated in the *FoxJ1*$^{-/-EGFP}$ domains. (**C**) Western blotting of immunoprecipitated γ-tubulin complexes from P6 mice revealed a potential interaction with Dnahc, Dnaic and Kif6 proteins in wild-type mice, and the absence of these complexes in the *FoxJ1*$^{-/-}$ brain.

The potential role of candidate genes in the generation of motile cilia in ependymal cells

The functional classification of the identified genes pointed to a master regulatory role for FoxJ1 in driving the expression of the motility apparatus within cilia in the mouse brain, as has been shown in *Xenopus* and zebrafish (Yu et al., 2008; Stubbs et al., 2008). To shed light on whether or not the significant downregulation of dynein and kinesin motor proteins was related to aggregation of γ-tubulin in the cytoplasm of *FoxJ1*$^{-/-}$ ependymal cells, we analyzed their expression and biochemical interactions in the brain. First, we found that most of the identified axonemal dynein and kinesin proteins had a restricted expression in the ependymal layer of the adult SVZ (see Fig. S9 in the supplementary material).

Next, to determine the potential interaction of identified proteins with γ-tubulin, total proteins from P6 wild-type and *FoxJ1*-null forebrains were extracted and γ-tubulin was immunoprecipitated. Western blotting was then performed on immunoprecipitated proteins to determine whether Dnahc, Dnaic and Kif6 were forming a complex with γ-tubulin. All three proteins were detected in immunoprecipitated wild-type extracts, indicating that they formed a complex with γ-tubulin at the peak of ependymal cell differentiation (Fig. 7C). By contrast, levels of all three proteins were extremely low or absent in *FoxJ1*$^{-/-}$ extracts and undetectable in γ-tubulin-immunoprecipitated material from *FoxJ1*$^{-/-}$ brains (Fig. 7C). These findings indicate that physical interactions among γ-tubulin, axonemal dyneins and specific isoforms of kinesin motor proteins may be responsible for the transport and distribution of basal bodies to the ventricular surface of ependymal cells prior to the genesis of motile cilia (Fig. 8).

DISCUSSION

The ependymal component of the postnatal stem cell niche is thought to be crucial for neurogenesis in the OB, but its precise role in the regulation of neurogenesis remains little studied. We found that ependymal cells within distinct anatomical regions of the ventricular zone appear to differentiate at distinct postnatal time-points within the walls of the ventricles. Ependymal cells in the striatal wall, which are components of a neural stem cell niche, differentiate later during postnatal periods than other ependymal cells in the medial or dorsal walls of the lateral ventricles. This finding indicates the potential existence of regionally distinct ependymal subtypes within the walls of the ventricles; however, we found that in the absence of FoxJ1 expression, all ependymal cells within the lateral ventricles fail to differentiate during postnatal periods, regardless of their position. We also discovered a small subset of FoxJ1-expressing astrocytes that appear late during the differentiation of the SCN, and that their cellular organization in the postnatal SVZ unequivocally relies on transcriptional activity by FoxJ1.

FoxJ1 belongs to a recently annotated class of transcription factors with at least 30 family members that share a common forkhead (Fox) DNA-binding domain (Lehmann et al., 2003; Katoh and Katoh, 2004). FoxJ1 plays a direct role in the development of motile cilia (Brody et al., 2000; Yu et al., 2008; Stubbs et al., 2008), and motile cilia are important elements of ependymal cell differentiation and function in the central nervous system (Spassky et al., 2005; Sawamoto et al., 2006). Our analyses demonstrate that FoxJ1-dependent differentiation in ependymal cells includes the expression of a significant number of cytoskeletal proteins associated with motile cilia, and indicate their potential role in regulating the transport of γ-tubulin-containing basal bodies to the apical surface of differentiating ependymal cells. Although the focus of this study was on FoxJ1-dependent expression of microtubule-associated proteins and their potential role in the transport of basal bodies, the list of identified genes included additional functional families (see Table S1 in the supplementary material). This finding suggests a potentially broader function for FoxJ1-dependent differentiation in the SCN than in just the genesis of motile cilia. The function of most of the identified genes in SCN differentiation remains to be elucidated.

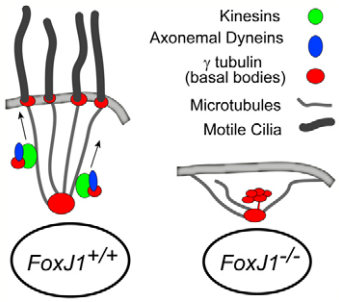

Fig. 8. Working model of the cell-autonomous function of FoxJ1 for genesis of motile cilia in ependymal cells. A physical interaction among γ-tubulin, dynein and kinesin motor proteins may regulate the transport of γ-tubulin rings (basal bodies) on the apical (ventricular) surface of ependymal cells. In the absence of FoxJ1, expression of these motor proteins is severely depleted, resulting in aggregation of γ-tubulin rings in *FoxJ1*$^{-/-}$ radial glia.

Cell-autonomous function of FoxJ1 in the genesis of motile cilia in ependymal cells

We demonstrated that, in the absence of FoxJ1, radial glia in the ventricular zone of the late embryonic brain fail to differentiate into ependymal cells. The unique molecular feature of *FoxJ1*-null cells includes intracellular accumulation of γ-tubulin protein, which is consistent with the previous finding of undocked γ-tubulin-containing basal bodies in multiciliated *FoxJ1*$^{-/-}$ lung epithelial cells (Brody et al., 2000; You et al., 2004). These findings suggest that generation of multiple basal bodies in multiciliated epithelial and ependymal cells is independent of FoxJ1 activity. FoxJ1-dependent docking of basal bodies has been linked to Ezrin-associated signaling (Gomperts et al., 2004) and Rho-mediated enrichment of actin (Pan et al., 2007) at the apical surface of airway epithelial cells. However, mechanisms of basal body transport prior to docking are still largely unknown. It is currently thought that this transport is mediated by the fusion of basal bodies to vesicles (Vladar and Axelrod, 2008), and no distinction has been made between transport of basal bodies for generation of motile versus primary cilia. Our finding that primary cilia are normal in the *FoxJ1*$^{-/-}$ brain is highly suggestive of divergent mechanisms of basal body transport for the genesis of motile and primary cilia.

The accumulation of γ-tubulin in *FoxJ1*$^{-/-}$ cells further suggests that replicated basal bodies may be distributed to the apical surface of ependymal cells utilizing proteins involved in intracellular transport, the expression of which depends on FoxJ1 activity. Hints toward potential mechanisms for this transport came from our transcriptome comparison of *FoxJ1*$^{-/-}$ and wild-type brains. Of the candidate genes downregulated in *FoxJ1*-null brains, a significant number are microtubule-associated proteins. In particular, three isoforms of kinesin motor proteins (Kif6/9/27) can be predicted to be responsible for transport of γ-tubulin and axonemal proteins to the apical (ventricular) surface of differentiating ependymal cells. In support of this possibility, we showed that Kif6 is found in a complex that includes γ-tubulin, Dnahc and Dnaic. Finally, the confined expression of the majority of the identified genes to the ependymal layer of the SVZ is highly suggestive of a direct role for FoxJ1 in the expression of the identified genes and their potential function in the generation of motile cilia. Thus, we propose that Kif6, and potentially Kif9 and Kif27, motor proteins could be responsible for the transport of basal bodies to the surface of differentiating ependymal cells (Fig. 7D). It will be intriguing to determine whether or not any vesicular proteins are part of this complex. The sequence of signaling and molecular events driven by FoxJ1-dependent transcriptional activity during ciliogenesis remains to be elucidated.

FoxJ1^{+} astrocytes in the SCN

We also discovered a small subset of FoxJ1^{+} astrocytes that emerge in the postnatal SCN around P21 in mice and gradually increase in density by 6 months of age in the wild-type SVZ. The emergence of these astrocytes between P19 and P21 is dependent on FoxJ1 expression as their density is severely depleted in the *FoxJ1*$^{-/-}$ SVZ. Recent studies have described the expansion of a unique set of astrocytes in the aged ependymal layer (Luo et al., 2006), a phenomenon later shown to be involved in the repair of ependymal cells in elderly mice (Luo et al., 2008). It is possible that the small population of resident FoxJ1^{+} astrocytes might participate in the repair of the aged ependymal layer. In support of this, recent studies have revealed that *FoxJ1* promoter-active cells in the spinal canal and SVZ participate in neurogenesis and gliogenesis in the injured spinal cord and in response to stroke (Meletis et al., 2008; Carlen et al., 2009). It will be intriguing to determine whether the shared expression of FoxJ1 by ependymal cells and a small subset of astrocytes is the basis of plasticity inherent to the adult SCN.

Although the cellular compartments of the adult SCN are fairly well characterized, the identity of adult neural stem cells has remained largely elusive. Our in vitro findings reveal that subsets of *FoxJ1*^{EGFP} cells harvested from the P21 SVZ generate neurospheres, can self-renew and have the potential to give rise to astrocytes, oligodendrocytes and neurons, thus functionally resembling adult neural stem cells. Together with previous studies demonstrating that ependymal cells are not capable of generating neurospheres (Doetsch et al., 1999a; Laywell et al., 2000; Capela and Temple, 2002), our in vitro results suggest that the small subset of FoxJ1^{+} astrocytes in the SVZ and FoxJ1^{+} progenitor-like cells in the RMS are likely to be the source of the stem cell properties detected in our neurosphere experiments. Thus, FoxJ1^{+} radial-glia-like cells prior to P21, and FoxJ1^{+} astrocytes after P21, may directly contribute to progenitor populations in the LGE and SVZ perinatally, thus functioning as a subset of adult stem cells in vivo. In further support of this possibility, we found a subset of FoxJ1^{+} astrocytes in the hippocampal dentate gyrus, where they may also function as a subset of adult neural stem cells. Although a recent study attempted to lineage-trace FoxJ1^{+} cells using viral vectors (Carlen et al., 2009), genetic lineage tracing will be required to conclusively determine whether any of the FoxJ1^{+} cell types identified in our study participate in early postnatal and adult neurogenesis.

In summary, this study demonstrates the cellular requirement for FoxJ1 in the differentiation of the ependymal layer within the central nervous system. The timing of this unique differentiation process is not uniform across all ventricular zones of the brain. The ependymal differentiation along the striatal walls of the ventricles, where neurogenesis persists throughout life, is delayed compared with other ventricular zones. Curiously, the *FoxJ1* promoter appears to be preferentially active at low levels during embryogenesis in the LGE and olfactory ventricular zone, whereas it is inactive in other neurogenic niches of the embryonic brain. The cluster of FoxJ1-dependent genes identified in this study appears to be highly focused on the regulation of microtubule-based intracellular transport. Our findings suggest that the expression of the identified genes might be related to the transport of replicated basal bodies to the apical surface of the differentiating ependymal cells during the genesis of motile cilia. The role of FoxJ1-dependent differentiation of the SCN in postnatal neurogenesis remains to be determined in vivo.

Acknowledgements

We thank M. Iyengar, A. Sheikh and J. Burroughs for technical assistance. M. Vernon from the Functional Genomic Core Facility at University of North Carolina conducted the microarray hybridizations and helped organize the data. D. Eisenstat (U. Manitoba) kindly provided the Dlx2 antibody. We thank J. Weimer, S. Magness, A. Barnes and J. Horowitz for comments and discussions during various stages of this work. This work was entirely supported by startup funds to H.T.G. from the College of Veterinary Medicine and Department of Molecular Biomedical Sciences at NCSU.

Supplementary material

Supplementary material for this article is available at http://dev.biologists.org/cgi/content/full/136/23/4021/DC1

References

Alvarez-Buylla, A. and Lim, D. A. (2004). For the long run: maintaining germinal niches in the adult brain. *Neuron* **41**, 683-686.

Bayer, S. A. (1983). 3H-thymidine-radiographic studies of neurogenesis in the rat olfactory bulb. *Exp. Brain Res.* **50**, 329-340.

DEVELOPMENT

Brody, S. L., Yan, X. H., Wuerffel, M. K., Song, S. K. and Shapiro, S. D. (2000). Ciliogenesis and left-right axis defects in forkhead factor HFH-4-null mice. *Am. J. Respir. Cell Mol. Biol.* **23**, 45-51.
Campbell, K. and Gotz, M. (2002). Radial glia: multi-purpose cells for vertebrate brain development. *Trends Neurosci.* **25**, 235-238.
Capela, A. and Temple, S. (2002). LeX/ssea-1 is expressed by adult mouse CNS stem cells, identifying them as nonependymal. *Neuron* **35**, 865-875.
Carlen, M., Meletis, K., Goritz, C., Darsalia, V., Evergren, E., Tanigaki, K., Amendola, M., Barnabe-Heider, F., Yeung, M. S., Naldini, L. et al. (2009). Forebrain ependymal cells are Notch-dependent and generate neuroblasts and astrocytes after stroke. *Nat. Neurosci.* **12**, 259-267.
Coskun, V., Wu, H., Blanchi, B., Tsao, S., Kim, K., Zhao, J., Biancotti, J. C., Hutnick, L., Krueger, R. C., Jr, Fan, G. et al. (2008). CD133+ neural stem cells in the ependyma of mammalian postnatal forebrain. *Proc. Natl. Acad. Sci. USA* **105**, 1026-1031.
Doetsch, F., Garcia-Verdugo, J. M. and Alvarez-Buylla, A. (1997). Cellular composition and three-dimensional organization of the subventricular germinal zone in the adult mammalian brain. *J. Neurosci.* **17**, 5046-5061.
Doetsch, F., Caille, I., Lim, D. A., Garcia-Verdugo, J. M. and Alvarez-Buylla, A. (1999a). Subventricular zone astrocytes are neural stem cells in the adult mammalian brain. *Cell* **97**, 703-716.
Doetsch, F., Garcia-Verdugo, J. M. and Alvarez-Buylla, A. (1999b). Regeneration of a germinal layer in the adult mammalian brain. *Proc. Natl. Acad. Sci. USA* **96**, 11619-11624.
Edgar, R., Dornrachev, M. and Lash, A. E. (2002). Gene Expression Omnibus: NCBI gene expression and hybridization array data repository. *Nucleic Acids Res.* **30**, 207-210.
Ghashghaei, H. T., Weber, J., Pevny, L., Schmid, R., Schwab, M. H., Lloyd, K. C., Eisenstat, D. D., Lai, C. and Anton, E. S. (2006). The role of neuregulin-ErbB4 interactions on the proliferation and organization of cells in the subventricular zone. *Proc. Natl. Acad. Sci. USA* **103**, 1930-1935.
Ghashghaei, H. T., Lai, C. and Anton, E. S. (2007a). Neuronal migration in the adult brain: are we there yet? *Nat. Rev. Neurosci.* **8**, 141-151.
Ghashghaei, H. T., Weimer, J. M., Schmid, R. S., Yokota, Y., McCarthy, K. D., Popko, B. and Anton, E. S. (2007b). Reinduction of ErbB2 in astrocytes promotes radial glial progenitor identity in adult cerebral cortex. *Genes Dev.* **21**, 3258-3271.
Gomperts, B. N., Gong-Cooper, X. and Hackett, B. P. (2004). Foxj1 regulates basal body anchoring to the cytoskeleton of ciliated pulmonary epithelial cells. *J. Cell Sci.* **117**, 1329-1337.
Gong, Q. and Shipley, M. T. (1995). Evidence that pioneer olfactory axons regulate telencephalon cell cycle kinetics to induce the formation of the olfactory bulb. *Neuron* **14**, 91-101.
Hinds, J. W. (1968a). Autoradiographic study of histogenesis in the mouse olfactory bulb. I. Time of origin of neurons and neuroglia. *J. Comp. Neurol.* **134**, 287-304.
Hinds, J. W. (1968b). Autoradiographic study of histogenesis in the mouse olfactory bulb. II. Cell proliferation and migration. *J. Comp. Neurol.* **134**, 305-322.
Jacquet, B. V., Patel, M., Iyengar, M., Liang, H., Therit, B., Salinas-Mondragon, R., Lai, C., Olsen, J. C., Anton, E. S. and Ghashghaei, H. T. (2009). Analysis of neuronal proliferation, migration and differentiation in the postnatal brain using equine infectious anemia virus-based lentiviral vectors. *Gene Ther.* **16**, 1021-1033.
Johansson, C. B., Momma, S., Clarke, D. L., Risling, M., Lendahl, U. and Frisen, J. (1999). Identification of a neural stem cell in the adult mammalian central nervous system. *Cell* **96**, 25-34.
Katoh, M. and Katoh, M. (2004). Human FOX gene family. *Int. J. Oncol.* **25**, 1495-1500.
Kuo, C. T., Mirzadeh, Z., Soriano-Navarro, M., Rasin, M., Wang, D., Shen, J., Sestan, N., Garcia-Verdugo, J., Alvarez-Buylla, A., Jan, L. Y. et al. (2006). Postnatal deletion of Numb/Numblike reveals repair and remodeling capacity in the subventricular neurogenic niche 2. *Cell* **127**, 1253-1264.
Laywell, E. D., Rakic, P., Kukekov, V. G., Holland, E. C. and Steindler, D. A. (2000). Identification of a multipotent astrocytic stem cell in the immature and adult mouse brain. *Proc. Natl. Acad. Sci. USA* **97**, 13883-13888.
Lehmann, O. J., Sowden, J. C., Carlsson, P., Jordan, T. and Bhattacharya, S. S. (2003). Fox's in development and disease. *Trends Genet.* **19**, 339-344.
Lim, D. A., Tramontin, A. D., Trevejo, J. M., Herrera, D. G., Garcia-Verdugo, J. M. and Alvarez-Buylla, A. (2000). Noggin antagonizes BMP signaling to create a niche for adult neurogenesis. *Neuron* **28**, 713-726.
Livak, K. J. and Schmittgen, T. D. (2001). Analysis of relative gene expression data using real-time quantitative PCR and the 2(-Delta Delta C(T)) method. *Methods* **25**, 402-408.
Lois, C. and Alvarez-Buylla, A. (1993). Proliferating subventricular zone cells in the adult mammalian forebrain can differentiate into neurons and glia. *Proc. Natl. Acad. Sci. USA* **90**, 2074-2077.
Lois, C. and Alvarez-Buylla, A. (1994). Long-distance neuronal migration in the adult mammalian brain. *Science* **264**, 1145-1148.
Luo, J., Daniels, S. B., Lennington, J. B., Notti, R. Q. and Conover, J. C. (2006). The aging neurogenic subventricular zone. *Aging Cell* **5**, 139-152.
Luo, J., Shook, B. A., Daniels, S. B. and Conover, J. C. (2008). Subventricular zone-mediated ependyma repair in the adult mammalian brain. *J. Neurosci.* **28**, 3804-3813.
Marlin, A. E., Wald, A., Hochwald, G. M. and Malhan, C. (1978). Kaolin-induced hydrocephalus impairs CSF secretion by the choroid plexus. *Neurology* **28**, 945-949.
Meletis, K., Barnabe-Heider, F., Carlen, M., Evergren, E., Tomilin, N., Shupliakov, O. and Frisen, J. (2008). Spinal cord injury reveals multilineage differentiation of ependymal cells. *PLoS Biol.* **6**, e182.
Merkle, F. T., Tramontin, A. D., Garcia-Verdugo, J. M. and Alvarez-Buylla, A. (2004). Radial glia give rise to adult neural stem cells in the subventricular zone. *Proc. Natl. Acad. Sci. USA* **101**, 17528-17532.
Mirzadeh, Z., Merkle, F. T., Soriano-Navarro, M., Garcia-Verdugo, J. M. and Alvarez-Buylla, A. (2008). Neural stem cells confer unique pinwheel architecture to the ventricular surface in neurogenic regions of the adult brain. *Cell Stem Cell* **3**, 265-278.
Mitchell, D. R. (2004). Speculations on the evolution of 9+2 organelles and the role of central pair microtubules. *Biol. Cell* **96**, 691-696.
Noctor, S. C., Flint, A. C., Weissman, T. A., Wong, W. S., Clinton, B. K. and Kriegstein, A. R. (2002). Dividing precursor cells of the embryonic cortical ventricular zone have morphological and molecular characteristics of radial glia. *J. Neurosci.* **22**, 3161-3173.
Nonaka, S., Tanaka, Y., Okada, Y., Takeda, S., Harada, A., Kanai, Y., Kido, M. and Hirokawa, N. (1998). Randomization of left-right asymmetry due to loss of nodal cilia generating leftward flow of extraembryonic fluid in mice lacking KIF3B motor protein. *Cell* **95**, 829-837.
O'Rourke, J. P., Olsen, J. C. and Bunnell, B. A. (2005). Optimization of equine infectious anemia derived vectors for hematopoietic cell lineage gene transfer. *Gene Ther.* **12**, 22-29.
Oakley, B. R. (1992). Gamma-tubulin: the microtubule organizer? *Trends Cell Biol.* **2**, 1-5.
Olsen, J. C. (1998). Gene transfer vectors derived from equine infectious anemia virus. *Gene Ther.* **5**, 1481-1487.
Ostrowski, L. E., Hutchins, J. R., Zakel, K. and O'Neal, W. K. (2003). Targeting expression of a transgene to the airway surface epithelium using a ciliated cell-specific promoter. *Mol. Ther.* **8**, 637-645.
Ostrowski, L. E., Yin, W., Rogers, T. D., Busalacchi, K. B., Chua, M., O'Neal, W. K. and Grubb, B. R. (2009). Conditional deletion of Dnaic1 in a murine model of primary ciliary dyskinesia causes chronic rhinosinusitis. *Am. J. Respir. Cell Mol. Biol*. (in press).
Pan, J., You, Y., Huang, T. and Brody, S. L. (2007). RhoA-mediated apical actin enrichment is required for ciliogenesis and promoted by Foxj1. *J. Cell Sci.* **120**, 1868-1876.
Pinto, L. and Gotz, M. (2007). Radial glial cell heterogeneity-the source of diverse progeny in the CNS. *Prog. Neurobiol.* **83**, 2-23.
Rakic, P. (1972). Mode of cell migration to the superficial layers of fetal monkey neocortex. *J. Comp. Neurol.* **145**, 61-83.
Reynolds, B. A. and Weiss, S. (1992). Generation of neurons and astrocytes from isolated cells of the adult mammalian central nervous system. *Science* **255**, 1707-1710.
Sawamoto, K., Wichterle, H., Gonzalez-Perez, O., Cholfin, J. A., Yamada, M., Spassky, N., Murcia, N. S., Garcia-Verdugo, J. M., Marin, O., Rubenstein, J. L. et al. (2006). New neurons follow the flow of cerebrospinal fluid in the adult brain. *Science* **311**, 629-632.
Schlessinger, K., Hall, A. and Tolwinski, N. (2009). Wnt signaling pathways meet Rho GTPases. *Genes Dev.* **23**, 265-277.
Schmechel, D. E. and Rakic, P. (1979). A Golgi study of radial glial cells in developing monkey telencephalon: morphogenesis and transformation into astrocytes. *Anat. Embryol. (Berl)* **156**, 115-152.
Spassky, N., Merkle, F. T., Flames, N., Tramontin, A. D., Garcia-Verdugo, J. M. and Alvarez-Buylla, A. (2005). Adult ependymal cells are postmitotic and are derived from radial glial cells during embryogenesis. *J. Neurosci.* **25**, 10-18.
Stubbs, J. L., Oishi, I., Izpisua Belmonte, J. C. and Kintner, C. (2008). The forkhead protein Foxj1 specifies node-like cilia in Xenopus and zebrafish embryos. *Nat. Genet.* **40**, 1454-1460.
Tavazoie, M., Van, d., V, Silva-Vargas, V., Louissaint, M., Colonna, L., Zaidi, B., Garcia-Verdugo, J. M. and Doetsch, F. (2008). A specialized vascular niche for adult neural stem cells. *Cell Stem Cell* **3**, 279-288.
Vladar, E. K. and Axelrod, J. D. (2008). Dishevelled links basal body docking and orientation in ciliated epithelial cells. *Trends Cell Biol.* **18**, 517-520.
Wichterle, H., Garcia-Verdugo, J. M., Herrera, D. G. and Alvarez-Buylla, A. (1999). Young neurons from medial ganglionic eminence disperse in adult and embryonic brain. *Nat. Neurosci.* **2**, 461-466.
You, Y., Huang, T., Richer, E. J., Schmidt, J. E., Zabner, J., Borok, Z. and Brody, S. L. (2004). Role of f-box factor foxj1 in differentiation of ciliated airway epithelial cells. *Am. J. Physiol. Lung Cell Mol. Physiol.* **286,** L650-L657.
Yu, X., Ng, C. P., Habacher, H. and Roy, S. (2008). Foxj1 transcription factors are master regulators of the motile ciliogenic program. *Nat. Genet.* **40**, 1445-1453.
Zallen, J. A. (2007). Planar polarity and tissue morphogenesis. *Cell* **129**, 1051-1063.

Table S1. Putative target genes regulated by FOXJ1 with confirmed expression in the SCN

Gene	Affymetrix Probe set ID	RefSeq Transcript ID (NCBI)	Chr	Biological Process(es)	Molecular Function(s)	Cell compartment(s)
Secreted factors						
Ttr	10454192	NM_013697	chr18	thyroid hormone generation // transport	hormone activity // steroid binding // retinal binding // retinol binding	extracellular region
Extracellular matrix						
Prelp	10357870	NM_054077	chr1	cell aging	protein binding	extracellular region // proteinaceous extracellular matrix
Membrane Associated Proteins						
Cldn2	10602033	NM_016675	chrX	calcium-independent cell-cell adhesion	structural molecule activity	tight junction // membrane // cell junction
Tm4sf1	10498273	NM_008536	chr3	---	---	membrane
Membrane Channels						
Clic6	10436958	NM_172469	chr16	transport // ion transport // chloride transport	voltage-gated ion channel activity	cytoplasm // membrane
Kcnj16	10382316	NM_010604	chr11	potassium ion transport	inward rectifier potassium channel activity	membrane
Sperm/flagellum/cilium Proteins						
Efhc1	10345046	EU520262	chr1	cellular calcium ion homeostasis // positive regulation of apoptosis	calcium ion binding	cilium // axoneme // flagellum // cell soma
Spag6	10438049	NM_015773	chr16	spermatogenesis // cell projection organization and biogenesis // sperm motility	binding	cytoplasm // cytoskeleton // microtubule // cilium // flagellum // cell projection
Spa17	10592336	NM_011449	chr9	signal transduction // binding of sperm to zona pellucida	cAMP-dependent protein kinase regulator activity	membrane
Spata17	10360942	NM_028848	chr1	spermatogenesis	calmodulin binding	cytoplasm
Spata18	10522445	BC050799	chr5	spermatogenesis	---	cytoplasm
Tsnaxip1	10574880	NM_024445	chr8	multicellular organismal development // spermatogenesis // cell differentiation	protein binding	cytoplasm
Calcium Binding Proteins						
Capsl	10423024	NM_029341	chr15	---	calcium ion binding	cytoplasm
Calml4	10586118	NM_138304	chr9	---	calcium ion binding	---
Efcab1	10433782	NM_025769	chr16	---	calcium ion binding	---
Efhb	10451786	NM_172497	chr17	---	calcium ion binding	---
Prrg4	10485624	NM_178695	chr2	---	calcium ion binding	extracellular region

Table S1. Putative target genes regulated by FOXJ1 with confirmed expression in the SCN

Kinase/Phosphatase Proteins						
Cdkl4	10453166	NM_001033443	chr17	protein amino acid phosphorylation	nucleotide binding // protein kinase activity // protein serine/threonine kinase activity // cyclin-dependent protein kinase activity // ATP binding // kinase activity // transferase activity	cytoplasm
Musk	10505145	NM_001037127	chr4	regulation of transcription, DNA-dependent // protein amino acid phosphorylation // neuromuscular junction development // regulation of synaptic growth at neuromuscular junction // receptor clustering // receptor clustering	protein serine/threonine kinase activity // protein tyrosine kinase activity // receptor activity // ATP binding // transferase activity	plasma membrane // integral to plasma membrane // membrane // integral to membrane // neuromuscular junction
Nek5	10577471	NM_177898	chr8	protein amino acid phosphorylation	nucleotide binding // magnesium ion binding // protein kinase activity // protein serine/threonine kinase activity // ATP binding // kinase activity // transferase activity // metal ion binding	---
Iqca	10356512	ENSMUST00000113094	chr1	---	nucleotide binding // ATP binding // nucleoside-triphosphatase activity	---
Ysk4	10357381	XM_914055	chr1	Homologue of Sps1/Ste20-related kinase 4 (Yeast)	---	---
Metabolic Proteins						
Apoe	10560624	NM_009696	chr7	lipid metabolic process // cholesterol catabolic process // transport // cellular calcium ion homeostasis // response to oxidative stress // regulation of gene expression // axon regeneration // vasodilation // artery morphogenesis	lipid transporter activity // lipoprotein binding // heparin binding // lipid binding // cholesterol transporter activity	extracellular region // extracellular space // chylomicron
Bbox1	10485700	NM_130452	chr2	carnitine biosynthetic process // oxidation reduction	iron ion binding // gamma-butyrobetaine dioxygenase activity // electron carrier activity // oxidoreductase activity	cytoplasm
Car9	10504337	NM_139305	chr4	morphogenesis of an epithelium // one-carbon compound metabolic process // secretion	carbonate dehydratase activity // zinc ion binding // lyase activity	membrane // cell projection
Cpn1	10467887	NM_030703	chr19	proteolysis	carboxypeptidase activity // metallopeptidase activity // zinc ion binding	extracellular region

Table S1. Putative target genes regulated by FOXJ1 with confirmed expression in the SCN

Dnajb13	10565890	NM_153527	chr7	protein folding	heat shock protein binding // unfolded protein binding	---
Enpp2	10428619	NM_015744	chr15	chemotaxis // lipid catabolic process	nucleic acid binding // endonuclease activity // phosphodiesterase I activity // nucleotide diphosphatase activity // hydrolase activity // metal ion binding // alkylglycerophosphoethanolamine phosphodiesterase activity	extracellular region // membrane
Folr1	10566034	NM_008034	chr7	posttranslational protein targeting to membrane // folic acid metabolic process	receptor activity // folic acid binding // folic acid transporter activity	membrane
Hspa8	10584572	NM_031165	chr9	protein folding // response to stress // chaperone cofactor-dependent protein folding // regulation of cell cycle	nucleotide binding // protein binding // ATP binding // ATPase activity // unfolded protein binding	cytoplasm
Mdh1b	10355121	NM_029696	chr1	carbohydrate metabolic process // tricarboxylic acid cycle // malate metabolic process // oxidation reduction	catalytic activity // oxidoreductase activity // malate dehydrogenase activity	---
Wdr66	10525516	BC138176	chr5	---	peptidase activity	---
Cytoskeletal/microtubule Associated Proteins						
Dynll1	10532984	NM_019682	chr5	microtubule-based process // microtubule-based movement // negative regulation of nitric oxide biosynthetic process	motor activity // microtubule motor activity // enzyme inhibitor activity	cytoplasm // cytoskeleton
Dynlrb2	10575725	NM_029297	chr8	---	motor activity	cytoplasm // cytoskeleton
Dnahc11	10403112	NM_010060	chr12	ciliary or flagellar motility // determination of left/right symmetry	nucleotide binding // microtubule motor activity // ATP binding	cilium
Dnahc12	10413333	ENSMUST00000073309	chr14	---	---	---
Dnahc3	10567446	BC051401	chr7	microtubule-based movement // biological_process	nucleotide binding // molecular_function // motor activity // microtubule motor activity // ATP binding // ATPase activity // nucleoside-triphosphatase activity	cytoskeleton // cilium
Dnahc5	10423388	NM_133365	chr15	ciliary or flagellar motility // microtubule-based movement	nucleotide binding // motor activity // microtubule motor activity // ATP binding // ATPase activity // nucleoside-triphosphatase activity	cytoskeleton // cilium
Dnahc6	10545502	ENSMUST00000114040	chr6	---	---	---
Dnahc9	10387029	NM_001099633	chr11	---	nucleotide binding // ATP binding	cilium

Table S1. Putative target genes regulated by FOXJ1 with confirmed expression in the SCN

Dnaic1	10504072	NM_175138	chr4	---	motor activity	cytoskeleton // cilium
Dnali1	10516259	NM_175223	chr4	---	motor activity	dynein complex
Kif27	10409666	NM_175214	chr13	microtubule-based movement	nucleotide binding // motor activity // microtubule motor activity // ATP binding	microtubule // microtubule associated complex
Kif6	10445839	NM_177052	chr17	---	nucleotide binding // motor activity // ATP binding	microtubule
Kif9	10589541	NM_010628	chr9	microtubule-based movement	nucleotide binding // motor activity // microtubule motor activity // ATP binding	microtubule // microtubule associated complex
Rshl3	10362472	BC138000	chr10	---	---	cilium (unconfirmed)
Tekt4	10442807	NM_027951	chr17	microtubule cytoskeleton organization and biogenesis // cell projection organization and biogenesis	structural molecule activity	microtubule // cilium // flagellum // cell projection
Tmod1	10504692	NM_021883	chr4	myofibril assembly // muscle thick filament assembly	actin binding // tropomyosin binding	cytoplasm // cytoskeleton // myofibril
Ttll6	10380599	NM_172799	chr11	protein modification process	tubulin-tyrosine ligase activity	cilium // cell projection
Nuclear Proteins						
Meig1	10479761	NM_008579	chr2	meiosis	protein binding	nucleus
Mns1	10586907	NM_008613	chr9	meiosis	---	nucleus // nuclear envelope // intermediate filament
Mlf1	10492469	NM_001039543	chr3	myeloid progenitor cell differentiation // transcription // cell cycle // cell differentiation	DNA binding // protein binding	nucleus // cytoplasm
Nek11	10596327	NM_172461	chr9	protein amino acid phosphorylation // cell cycle	nucleotide binding // protein kinase activity // protein serine/threonine kinase activity // transferase activity // metal ion binding	nucleus
Syne1	10361381	NM_001079686	chr10	biological_process	actin binding // protein binding	nuclear envelope // sarcomere

Table S1. List of 55 characterized genes consistently and significantly down regulated in the *FoxJ1 null* SCN during early postnatal development (P1-P14). Expression of these genes in the ependymal layer of the SVZ and in the RMS was confirmed in the Allen Brain Atlas (http://mouse.brain-map.org/); Chr, chromosome; ---, information not available or unknown.

Table S2. Primers used for qRT-PCR verification of selected genes from microarray experiments and internal control genes

Gene	Forward primer (5′-3′)	Reverse primer (5′-3′)
FoxJ1	ACCCTACTCCTATGCCACTCTCAT	TGCATGGCGGAAGTAGCAGAAGTT
Dnahc3	ACTCGTCTGAGGAATCCACATT	GTACTCGATCCGTAAATCCAGC
Dnahc5	CTCTGTCAGTGCTGGGCATA	AAGAAATGCAGGAGTCAGCC
Dnahc6	GTAACCAATGAGCCTCCAAAAG	GGAACTCTGGTCTGGATTGAAG
Dnahc9	TTGCCTTGCTTCTCCAGATT	AATCTATCACCCACCACCCA
Dnahc11	GGAAGACCTCCGTTACCTCTTT	GAGTCCAAGTATCAAGTTCCCG
Dnahc12	GTGTAGTGTTCAATTGCTCCGA	TCGAAGAAGCAGTATGTCCTCA
Dnaic1	CACTGCCTTTGACTTCCACA	CACAGCGTCTACTGCCATGT
Dnali1	ACTCCCAGTGTTTTGACGAACT	GTTAGTGAGATGACAAAGCCCC
Dynlrb2	CCTCCTGACGATACCTGGAA	ATCCCTGACTGTGCTCTTGG
Dynll1	GCTTCTTACGGAGAGCCTCA	GCACACACCAACAGCAAAGT
Tekt4	GAACACCAGATTGCAGCCTT	AACCTGAACTGGGCATTGTC
Kif6	CTCTGGGGAAAGTGACCAAC	CTTGGTCTTCCAAATAGGATGC
Kif27	GCGAGAAACGGAACGTAAAC	CTTTTGCTGGAGGGTCAGTC
Kif9	AAGACTCCTTAGGGGGAAACTG	GTCTTTGAGATCCCCATCTTTG
Ttll6	ATTCGCCAGTGGAAGAGAGA	CCAGCAAGACTGAAGGGAAG
Rshl3	CAAGCCCACCACCAGTTTAT	TGTGTCATCCTGAAAGCCTG
Internal controls		
TransfRec (signal: 25-75)	TTCCGCTCGTGGAGACTACT	ACATAGGGCGACAGGAAGTG
Pcx (signal: 100-200)	CTGGCAGGTAGTTGCTCACA	GGTAGAAGCCCTAAGCCACC
MUR_b2 (signal: 600-1000)	AAAACATGGGCTGGTGAGAT	TGGTTGCTGGGATTTGAACT
18SrRNA (signal: 6000-9000)	CGAAAGCATTTGCCAAGAAT	AGTCGGCATCGTTTATGGTC
GAPDH (signal: 10,000-15,000)	TGTTCCTACCCCCAATGTGT	GAGTTGCTGTTGAAGTCGCA
B2-element (signal: 14,000-20,000)	CAAAAATCTGATGCCCTGGT	GGGGAATAATGCTTCAGTGG